Ideal interchange instabilities in stellarators with a magnetic hill

T. Tatsuno*, M. Wakatani
Graduate School of Energy Science, Kyoto University,
Kyoto, Japan

K. Ichiguchi
National Institute for Fusion Science,
Oroshi-cho, Toki, Japan

Abstract. The prediction of the Mercier (Suydam) criterion for localized interchange modes in stellarators shows stability in cases in which global modes are unstable. One case is non-resonant pressure driven instabilities with low mode numbers which become unstable even if the mode resonant surface does not exist inside the plasma column. The other case is interchange instabilities when the pressure gradient vanishes at the mode resonant surface. If the pressure becomes flat in a narrow region around the mode resonant surface, high mode number instabilities are suppressed and the beta limit at the particular resonant surface increases. The radial mode structure at nearly marginal beta also changes significantly. The properties of the non-resonant mode and the transition from a resonant to a non-resonant mode are clarified with a cylindrical plasma model for a low shear stellarator with a magnetic hill.

1. Introduction

Although the Mercier criterion is useful for investigating pressure driven instabilities in tokamaks [1] and stellarators [2], it does not predict the limiting conditions in some cases within the ideal MHD model. For deriving the Mercier criterion it is assumed that the unstable mode is radially localized near the mode resonant surface. There is a tendency for the radial mode structure to become narrow in the vicinity of the mode resonant surface with an increase of mode number. Even the interchange mode with ($m = 1$, $n = 1$) has the property that the radial mode structure becomes highly localized near the marginal regime [3], where $m(n)$ is the poloidal (toroidal) mode number. This result explains why the Mercier limit correlates with the beta limit due to the interchange instabilities with low mode numbers [4, 5]. However, this situation changes substantially when the pressure gradient becomes locally flat at the mode resonant surface [6]. Details of the effect of pressure profile on the interchange modes will be given in this article with the use of a cylindrical plasma model for a low shear stellarator with a magnetic hill.

In order to destabilize the interchange mode, a resonant surface is not always necessary. It is reasonable that in a low shear region, with a steep pressure gradient, non-resonant modes approximately satisfying the resonant condition are destabilized. First, unstable non-resonant resistive modes were found for a Heliotron-E plasma with a highly peaked pressure profile [7]. Recently, ideal non-resonant modes were shown to be unstable in the central region of Heliotron-E [8], which seems consistent with the ($m = 2$, $n = 1$) mode triggering a sawtooth [9]. It is noted that non-resonant modes usually have global mode structures, which requires numerical analysis to clarify their properties. For studying the details of ideal non-resonant instabilities we use a cylindrical plasma model which saves computational time greatly. Since it is hard to excite a non-resonant mode in a high shear region, our interest is in a low shear stellarator with a magnetic hill.

It is noted that Fu et al. [5] studied the relation between Mercier modes and low-n modes with a full 3-D stability code for $l = 2$ stellarators. They found that unstable localized low-n modes are correlated with the Mercier criterion. However, the stability of global type low-n modes was found to be decorrelated from that of Mercier modes for the case with a fairly large outward magnetic axis shift. It seems that strong poloidal coupling in the toroidal geometry is essential for this type of unstable mode, which may

* *Present affiliation:* Graduate School of Frontier Sciences, University of Tokyo, Tokyo, Japan. E-mail: tatsuno@plasma.q.t.u-tokyo.ac.jp

be a tokamak type ballooning mode. In this article our interest is in the decorrelation between the low-n pressure driven modes and the Suydam modes in the cylindrical model. Thus, both the rotational transform and the pressure profiles are important here.

In Section 2, we derive an eigenmode equation for studying linear interchange modes in stellarators, which is derived from the reduced MHD equations [10]. In Section 3, we first solve the eigenmode equation analytically in the low shear limit, and discuss the non-resonant mode. Next, we solve the same eigenvalue equation numerically for the finite shear case in Section 4. Here we give examples to highlight various properties for both the resonant and non-resonant modes. Finally, in Section 5, we summarize the results obtained and give some physical interpretations for the behaviour of the non-resonant mode.

2. Eigenmode equations

For analysing pressure driven instabilities in stellarators, we use the ideal reduced MHD equations [10], which are written as

$$\frac{\partial \psi}{\partial t} = \boldsymbol{B}\cdot\boldsymbol{\nabla} u \tag{1}$$

$$\rho\,\frac{d\,\nabla_\perp^2 u}{dt} = -\boldsymbol{B}\cdot\boldsymbol{\nabla} J_z + \boldsymbol{\nabla}\Omega\times\boldsymbol{\nabla} p\cdot\boldsymbol{e}_z \tag{2}$$

$$\frac{dp}{dt} = 0 \tag{3}$$

where

$$\boldsymbol{B}\cdot\boldsymbol{\nabla} = B_0\,\frac{\partial}{\partial z} + \boldsymbol{\nabla}\psi\times\boldsymbol{e}_z\cdot\boldsymbol{\nabla} \tag{4}$$

$$\frac{d}{dt} = \frac{\partial}{\partial t} + \boldsymbol{\nabla} u\times\boldsymbol{e}_z\cdot\boldsymbol{\nabla} \tag{5}$$

$$\Omega = \frac{2r\cos\theta}{R_0} + \frac{\overline{(\nabla\phi)^2}}{B_0^2} \tag{6}$$

$$J_z = -\nabla_\perp^2 A_z \tag{7}$$

$$A_z = \psi + \frac{1}{2B_0}\,\overline{\boldsymbol{\nabla}\langle\phi\rangle\times\boldsymbol{\nabla}\phi}\cdot\boldsymbol{e}_z. \tag{8}$$

Here ψ, u and Ω denote the poloidal flux function, the stream function and the average curvature of the magnetic field, respectively. The quasi-toroidal coordinates are introduced and the metric is written as

$$dl^2 = dr^2 + r^2 d\theta^2 + (R_0 + r\cos\theta)^2\,d\zeta^2 \tag{9}$$

where R_0 denotes the major radius of the torus, r the minor radius, and θ and $\zeta = z/R_0$ the poloidal and toroidal angle, respectively. Here a perfectly conducting wall is placed at the plasma boundary, and the boundary conditions are given by $B_r = \partial\psi/\partial\theta = 0$, $v_r = \partial\phi/\partial\theta = 0$ and $p = 0$ at $r = a$.

In the following study, we neglect the toroidal effect in the reduced MHD equations. We also assume that the equilibrium quantities do not depend on the poloidal angle θ. This assumption means that the flux surfaces have a circular cross-section in the large aspect ratio limit. Then the rotational transform is written as

$$\iota(r) \equiv \frac{R_0}{rB_0}\,\frac{d\psi_0}{dr} \tag{10}$$

where the equilibrium poloidal flux function is given by $\psi_0(r)$. Since the correction due to the diamagnetic current becomes higher order in this formulation, the rotational transform in this approximation includes only the vacuum helical field contribution.

For the stability analysis, we use the following normalization for the variables:

$$\psi \to aB_0\psi,\quad u \to \frac{aR_0}{\tau_{PA}}\,u,\quad t \to \tau_{PA}t$$

$$p \to p_0(r=0)p,\quad r \to ar,\quad J_z \to \frac{B_0}{\mu_0 a}\,J_z$$

$$\nabla_\perp^2 u \to \frac{R_0}{a\tau_{PA}}\,\nabla_\perp^2 u,\quad A_z \to aB_0 A_z \tag{11}$$

where $\tau_{PA} = R_0\sqrt{\mu_0\rho}/B_0$ denotes the poloidal Alfvén time and a the minor radius of the plasma column. Then the linearized reduced MHD equations can be written as

$$\gamma(\nabla_\perp^2 u) = -\frac{n-m\iota}{\gamma}\,\nabla_\perp^2[(n-m\iota)u] - \frac{D_s}{\gamma}\,\frac{m^2}{r^2}\,u \tag{12}$$

where D_s and the averaged helical curvature Ω are expressed as

$$D_s = -\frac{\beta_0}{2\epsilon^2}\,p'\Omega' \tag{13}$$

$$\Omega = \epsilon^2 N\left(r^2\iota + 2\int r\iota\,dr\right). \tag{14}$$

Here $\epsilon \equiv a/R_0$ denotes the inverse aspect ratio, $\beta_0 \equiv 2\mu_0 p_0(r=0)/B_0^2$ the central plasma beta value and N the toroidal period number of the helical field. In order to derive Eq. (12), all perturbed quantities are assumed to be proportional to

$\exp[\gamma t - \mathrm{i}(m\theta + n\zeta)]$. In Eq. (13), the prime denotes the derivative with respect to the normalized minor radius r. The perpendicular Laplacian operator in Eq. (12) is expressed as

$$\nabla_\perp^2 = \frac{1}{r}\frac{d}{dr}\left(r\frac{d}{dr}\right) - \frac{m^2}{r^2}. \tag{15}$$

Then the ordinary differential equation (12) for the stream function u with mode numbers (m, n) is written as

$$\frac{d^2u}{dr^2} + \left(\frac{1}{r} - \frac{2m\iota'(n - m\iota)}{\gamma^2 + (n - m\iota)^2}\right)\frac{du}{dr} - \left\{\frac{m^2}{r^2} + \frac{1}{\gamma^2 + (n - m\iota)^2} \times \left[\left(\frac{m\iota'}{r} + m\iota''\right)(n - m\iota) - \frac{D_s m^2}{r^2}\right]\right\} u = 0 \tag{16}$$

which is an eigenmode equation with eigenvalue γ^2.

For solving Eq. (16) the boundary condition at the plasma surface $r = 1$ is $u = 0$ under a fixed boundary condition. We also impose regularity of the solution at $r = 0$. With these boundary conditions, we can set up an eigenvalue problem for the eigenvalue or growth rate γ^2 and the corresponding eigenfunction u.

3. Analytic solution of eigenmode

In this section we assume $\iota' = 0$ for obtaining an analytic solution, then Eq. (16) is written as

$$\frac{d^2u}{dr^2} + \frac{1}{r}\frac{du}{dr} + \frac{m^2}{r^2}\left(\frac{D_s}{\gamma^2 + (n - m\iota)^2} - 1\right) u = 0. \tag{17}$$

For the parabolic pressure profile, $p = p_0(1 - r^2)$, the analytic solution is readily obtained with the transformation $\tilde{r} \equiv \{\tilde{D}_s m^2/[\gamma^2 + (n - m\iota)^2]\}^{1/2} r$, where $\tilde{D}_s = 4\beta_0 N\iota$. From the solution $u \propto J_m(\tilde{r})$ for the (m, n) mode and the boundary condition $u = 0$ at $r = 1$, the growth rate is written as

$$\gamma^2 = \frac{\tilde{D}_s m^2}{Z^2(m, k)} - (n - m\iota)^2 \tag{18}$$

where $Z(m, k)$ is the kth zero point of the mth order Bessel function of the first kind $J_m(\tilde{r})$.

Although the resonant surface does not exist inside the plasma column, it is seen that the mode satisfying $n \simeq m\iota$ is most unstable and that the unstable mode has a global structure without localization in the radial direction unlike the resonant mode. Further we notice that, when there is no magnetic shear, the radial mode structure, $J_m(Z(m, k)r)$, is not affected by the beta value. We notice from Eq. (18) that the more unstable mode has the smaller node number, and the eigenvalue is discrete with respect to k for the specified (m, n). This property is general and can be also shown even for the case with the method given by Goedbloed and Sakanaka [11] by writing the eigenmode equation (16) in the Sturmian form (Appendix). Since the LHS of Eq. (18) is proportional to γ^2 and the RHS is linear with respect to the plasma beta, the relation (18) gives a parabolic line in the (β, γ) plane. Thus a small variation in β_0 from marginal equilibrium may cause an abrupt increase of growth.

The beta limit for stability is obtained by substituting $\gamma^2 = 0$ into Eq. (18), which yields

$$\beta_{0c} = \frac{Z^2(m, k)(n - m\iota)}{4N\iota m^2}. \tag{19}$$

In order to examine the beta limit of the higher harmonic modes with the same helicity, we use the transformation of the variables $(m, n) \mapsto l(m, n)$, which yields

$$\beta_{0c}^l = \frac{Z^2(lm, k)(n - m\iota)}{4N\iota m^2}. \tag{20}$$

Since $Z(lm, k) > Z(m, k)$ for $l \geq 2$, the beta limit of the higher harmonic mode, β_{0c}^l, is higher than that for the $l = 1$ case, β_{0c}. This is different from the resonant modes with the same helicity, which give the same beta limit given by the Suydam criterion [3].

4. Numerical solution of eigenmode equation

4.1. Resonant and non-resonant modes for standard pressure profiles

We have solved Eq. (16) numerically by the 'shooting' method using the fourth order Runge–Kutta formula. At first we tried the same eigenvalue problem as that shown in Section 3 in order to validate the numerical code. The growth rates obtained for the $(m, n) = (2, 1)$ mode coincide well with the analytic solution, Eq. (18), and the radial mode structures described by the Bessel function $J_2(\tilde{r})$ seem to be unchanged by variation of β_0.

Next we have investigated the effect of magnetic shear on non-resonant modes for the standard

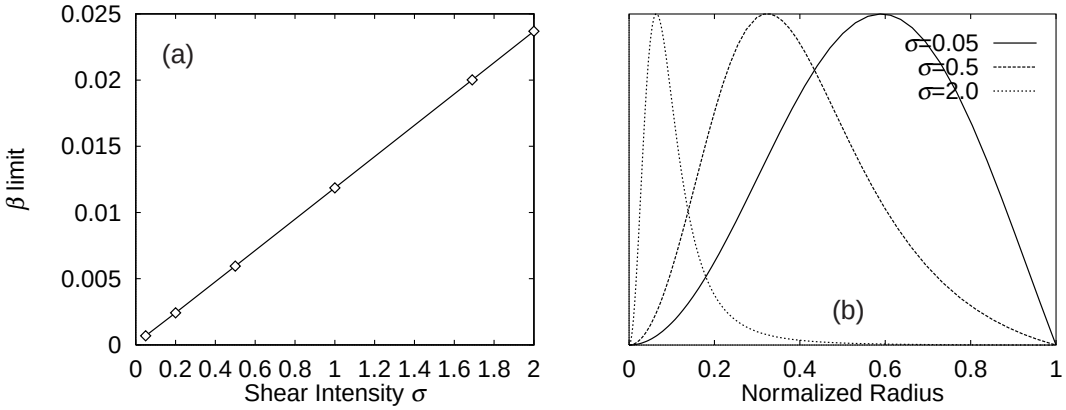

Figure 1. (a) Dependence of the beta limit on the magnetic shear parameter σ for the non-resonant $(2,1)$ mode. (b) Radial mode structures in the cases of $\sigma = 0.05$, 0.5 and 2.0 for a parabolic pressure profile with $\beta_0 = 0.03$.

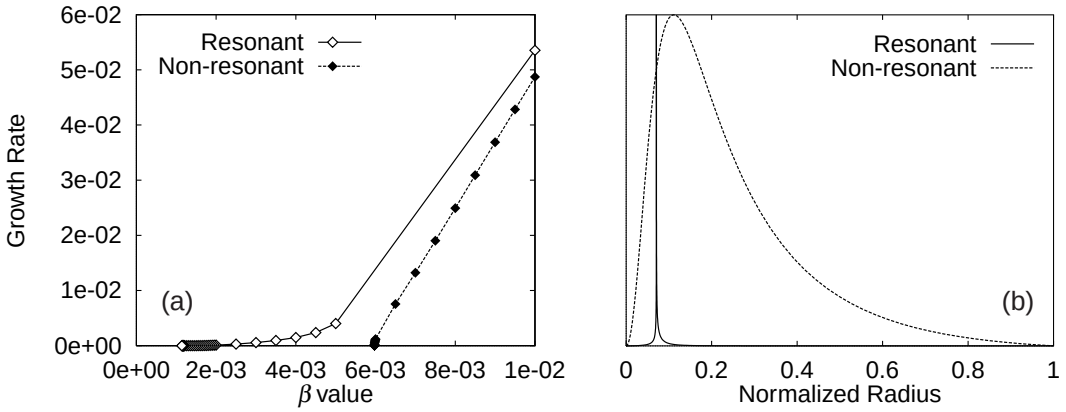

Figure 2. (a) Dependence of the growth rate of the $(2,1)$ mode on the central beta value β_0 for $p = p_0(1-r^4)$. Diamonds denote numerical results. The white diamonds correspond to the resonant case and the black diamonds to the non-resonant case. (b) Radial mode structures corresponding to the resonant ($\beta_0 = 1.35 \times 10^{-3}$) and non-resonant ($\beta_0 = 5.97 \times 10^{-3}$) cases. Here the rotational transform profile is $\iota(r) = 0.499 + 0.2r^2$ for the resonant case and $\iota(r) = 0.501 + 0.2r^2$ for the non-resonant case.

parabolic pressure profile. For the assumed rotational transform profile, $\iota = 0.51 + \sigma r^2$, σ is changed from 0.05 to 2.0. The rotational transform profile in the case of $\sigma = 1.69$ is approximately coincident with that in Heliotron-E [8]. When the beta value is fixed, the growth rate of the non-resonant $(2,1)$ mode is decreased with the increase of the magnetic shear intensity σ or the beta limit is increased almost linearly with the increase of σ, as shown in Fig. 1. The radial mode structure is shifted to the inner region when σ is increased (Fig. 1). This result can be interpreted in the following way. As σ is increased, there are two effects. First, the magnetic shear becomes larger in the outer region compared with the inner region. Second, the outer region is removed further away from the resonance than the inner region. These effects may account for the mode structure becoming more localized towards the magnetic axis. Also when β_0 is decreased, since the destabilizing effect due to the plasma pressure gradient becomes weak, the non-resonant mode can be excited only in the inner region. However, since there is no resonant surface, the radial mode structure is not highly localized and still has a global structure. The behaviour of the growth rate near the marginal beta value for the non-resonant mode is different from that for the resonant mode, as shown in Fig. 2. The growth rate of the non-resonant mode decreases to zero without

the tail at $\beta_0 \simeq \beta_{0c}$, where β_{0c} is the beta limit for the non-resonant $(2,1)$ mode.

Here we study the transition from the resonant mode to the non-resonant one. For currentless plasmas in Heliotron-E, MHD equilibria show that the central rotational transform is increased with an increase of beta value. When the vacuum rotational transform at the plasma centre is lower than 0.5, a resonant surface for the $(2,1)$ mode exists inside the plasma column. The resonant mode may not be excited due to the low beta value at the initial state. Experimental results show that the $(2,1)$ mode becomes unstable for $\beta_0 \gtrsim 0.7\%$ in neutral beam heated plasmas, which leads to the occurrence of sawtooth [8]. However, when ECRH is applied to the central region, the pressure profile becomes more peaked and the $(2,1)$ mode is stabilized. These data could be understood with the disappearance of the $\iota = 0.5$ surface according to the increase of the central beta value. Linear stability of the ideal $(2,1)$ mode in toroidal geometry shows that a resonant mode appears first, which then changes to a non-resonant mode with an increase of β_0. Finally, the non-resonant mode becomes stable, when $\iota(0)$ deviates far from 0.5 [8].

In the cylindrical model we simulate the above situation by changing the central value of the rotational transform artificially. To clarify the properties of the non-resonant mode, we consider a weak shear configuration with the resonant surface for the $(2,1)$ mode at first. Then we exclude the resonant surface of $\iota = 0.5$ by increasing $\iota(0)$. Figure 2 shows numerical results for the pressure profile $p = p_0(1 - r^4)$. White diamonds correspond to the growth rates for the equilibria with rotational transform profile $\iota = 0.499 + 0.2r^2$, which has the resonant surface for the $(2,1)$ mode at the normalized radius $r \simeq 0.07$. Black diamonds correspond to the growth rates for the equilibria with $\iota = 0.501 + 0.2r^2$, which has no resonant surface for the $(2,1)$ mode. The beta limit for the resonant case seems to be 1.14×10^{-3} or less, while for the non-resonant mode it is 5.97×10^{-3}. The difference between these beta limits correlates with the radial mode structure. In the small growth rate regime, when β_0 is decreased, the radial mode structure of the resonant mode becomes more localized. Thus, a highly localized mode with an extremely small growth rate is possible, as shown in Fig. 2. Thus, in β–γ space the line for the resonant mode case extends to the lower beta region with small growth rates. On the contrary, since the non-resonant mode cannot be localized at a particular surface, the growth rate decreases to zero without a tail with the decrease of β_0.

We can apply the Suydam criterion to resonant modes, which can be derived from the indicial equation of Eq. (16) at the singular point, or the resonant surface. It is written as

$$\frac{D_s}{\iota'^2 r_s^2} < \frac{1}{4} \tag{21}$$

for the stability case, where D_s and ι' are evaluated at the resonant surface, $r = r_s$, for the corresponding mode. In the case of Fig. 2, the resonant surface of the $(2,1)$ mode is $r_s \simeq 0.07$. Here the beta limit obtained from the criterion (21) is $\beta_0 \simeq 1.05 \times 10^{-3}$. Generally it is difficult to obtain the beta limit for the resonant mode numerically. One reason is the extension of the growth rate to the low beta side as mentioned above, and the other is the localization of the mode structure in the vicinity of the resonant surface. In Fig. 2, however, the difference between the analytic evaluation and the numerical result is less than 10%, and the growth rate at the numerically obtained beta limit is 4.49×10^{-11}, which is normalized by the poloidal Alfvén time.

It is noted that global type modes in toroidal stellarators are discussed in Ref. [5]. However, these modes are different from the non-resonant modes discussed here, since in toroidal geometry the poloidal coupling is essential to destabilize global type modes.

4.2. Resonant modes for locally flattened pressure profiles at the resonant surface

Here we consider the equilibria with resonant surface at $\iota = 0.5$ for the $(2,1)$ mode in the plasma column, but without the pressure gradient on the resonant surface. In the experimental situation of Heliotron-E, there may exist small magnetic islands due to resistive interchange instabilities at the low order resonant surfaces [12, 13], which may be nonlinearly saturated at low fluctuation levels. In such a case the equilibrium may not be violated by the resistive mode; however, the local plasma profile will change and the pressure gradient becomes small near the resonant surface [8, 14]. For this situation the Suydam criterion (21) predicts stability at the $\iota = 0.5$ surface. Here we will show that low-m modes can be unstable due to the finite negative pressure gradient at locations other than the resonant surface.

For simplicity the pressure profile is assumed to be

$$p = 1 - r^2 + \lambda(r - r_s)\exp\left[-\frac{1}{2}\left(\frac{r - r_s}{W}\right)^2\right] \qquad (22)$$

where r_s is the position of the mode resonant surface, and the choice $\lambda = 2r_s$ makes p' vanish at $r = r_s$. The width of the flat region is controlled with the parameter W. Several pressure profiles given by Eq. (22) are shown in Fig. 3. We assume $\iota = 0.45 + 0.2r^2$ and consider the $(2, 1)$ mode again. The resonant surface exists at $r_s = 0.5$ where the pressure gradient vanishes.

For the three cases with $W = 0$, 0.01 and 0.1 shown in Fig. 3, growth rates of the $(2, 1)$ mode are shown as a function of β_0 in Fig. 4(a). Although the highly localized mode structure is observed in the case of $W = 0$, it is not localized even in the case of $W = 0.01$, and the beta limit is increased by a factor of 2. Furthermore, in Fig. 4(a) the growth rate decreases to zero without a tail near the beta limit for $W = 0.01$, while the growth rate in the higher beta regime is not affected. The growth rates and the radial mode structures in the case of $W = 0.1$ are shown separately in Fig. 5, where both the first growing mode with the maximum growth rate and the second growing mode with the next growth rate are shown. In Figs 4(b) and 5(b) we see that the radial mode structures are quite different from the case with $W = 0$. They are restricted to one side of the mode resonant surface and change sharply at the mode resonant surface in the case of $W \neq 0$. In order to understand the role of the second growing mode, it is interesting to study the non-linear behaviour of the $(2, 1)$ mode for an equilibrium with a flat pressure region in the neighbourhood of the resonant surface. It is considered that, since the average magnetic shear is weak on the inner side of the resonant surface, the first growing mode is restricted to the region $[0, r_s]$ in the case of $W = 0.01$, whereas in the case of $W = 0.1$, it is restricted to the outer region since the average pressure gradient seems larger on the outer side. It is noted that the beta limit of the $W = 0.01$ case, $\beta_{0c} = 1.0 \times 10^{-3}$, is lower than that of the $W = 0.1$ case, $\beta_{0c} = 2.7 \times 10^{-3}$. In both cases the second growing mode appears in the opposite region to the first growing mode.

To investigate why the steep mode structure appears at the resonant surface, we expand the coefficients in Eq. (16) in the neighbourhood of the mode resonant surface $r = r_s$. Since the rotational transform is expanded as $\iota(r) \approx \iota(r_s) + \iota'(r_s)(r - r_s) + \ldots$, the resonant denominator is expressed as

$$n - m\iota \approx -m\iota'(r_s)(r - r_s) + \ldots . \qquad (23)$$

Since the pressure becomes flat at the mode resonant surface, $p'(r_s)$ becomes zero, but $p'(r)$ is still negative on both sides of the mode resonant surface. Therefore p'' is also zero at $r = r_s$, thus p' is expanded in the neighbourhood of the mode resonant surface as

$$p' \approx \frac{p'''(r_s)}{2}(r - r_s)^2 + \ldots \qquad (24)$$

where $p'''(r_s) < 0$. Substituting the leading terms of Eqs (23) and (24) into Eq. (16) yields

$$\frac{d^2u}{dr^2} + \left(\frac{1}{r} + \frac{2m^2\iota'^2(r - r_s)}{\gamma^2 + m^2\iota'^2(r - r_s)^2}\right)\frac{du}{dr} - \left[\frac{m^2}{r^2} - \frac{m\iota'(r - r_s)}{\gamma^2 + m^2\iota'^2(r - r_s)^2}\left(\frac{m\iota'}{r} + m\iota''\right) + \frac{m^2\beta_0 N p'''(4r_s\iota + r_s^2\iota')}{4r_s^2[\gamma^2 + m^2\iota'^2(r - r_s)^2]}(r - r_s)^2\right]u = 0. \qquad (25)$$

As seen here, the effect of the pressure near the resonant surface appears in higher order with respect to $r - r_s$. Thus, the pressure is negligible and does not affect the steep mode structure.

In order to confirm this situation, we have calculated the radial mode structure of the nearly marginal mode for the following pressure profiles numerically. One profile is

$$p = \begin{cases} \dfrac{1}{2}(1 - 4r^2)^2 + 0.5, & r < 0.5 \\ \dfrac{1}{2}[1 - 4(r - 0.5)^2]^2, & r > 0.5 \end{cases} \qquad (26)$$

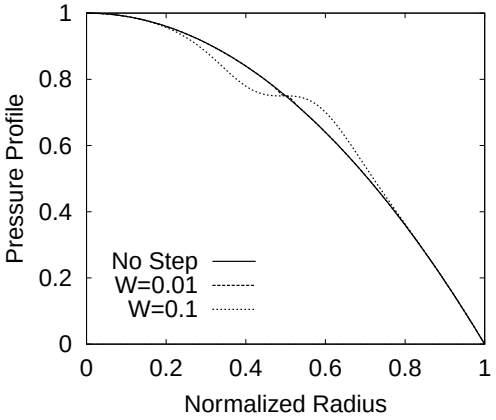

Figure 3. Pressure profiles given by Eq. (22) for $\lambda = 1$. The effect of pressure flattening is very small and visible only at $r \simeq 0.5$ for $W = 0.01$.

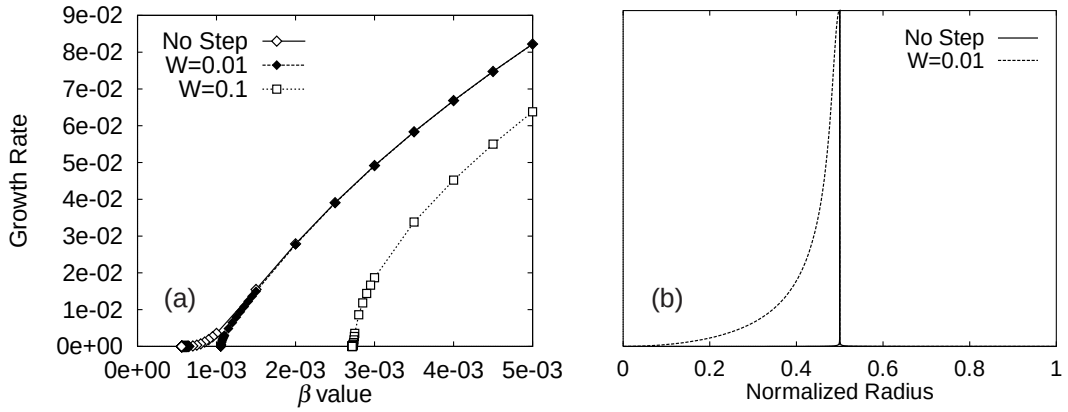

Figure 4. (a) Dependence of the growth rate of the $(2,1)$ mode on the central beta value β_0 for $W = 0$, 0.01 and 0.1. (b) Radial mode structures for $W = 0$ ($\beta_0 = 5.62 \times 10^{-4}$) and $W = 0.01$ ($\beta_0 = 1.05 \times 10^{-3}$). The radial mode structures for $W = 0.1$ are shown in Fig. 5.

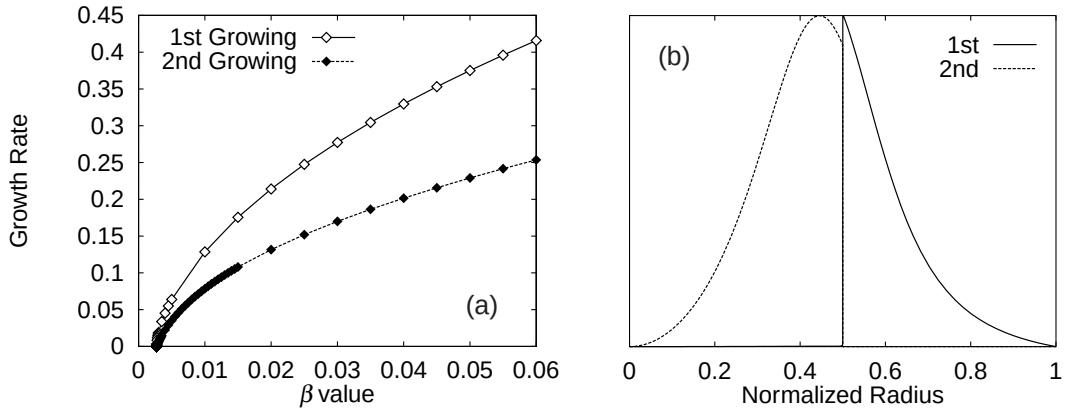

Figure 5. (a) Dependence of the growth rate of the $(2,1)$ mode on the central beta value β_0 for $W = 0.1$. (b) Radial mode structure of the first growing mode ($\beta_0 = 2.72 \times 10^{-3}$) and that of the second growing mode ($\beta_0 = 2.76 \times 10^{-3}$). It is noted that the growth rates of the first growing mode are the same as those in Fig. 4(a).

and the other is

$$p = \begin{cases} \frac{1}{2}\left(1 - \frac{25}{4}\,r^2\right)^2 + 0.5, & r < 0.4 \\ 0.5, & 0.4 < r < 0.6 \\ \frac{1}{2}\left[1 - \frac{25}{4}\,(r-0.6)^2\right]^2, & r > 0.6. \end{cases} \quad (27)$$

The latter pressure profile contains a completely flat region whose width is noted as δ in $[0.4, 0.6]$ in order to eliminate the effect of the pressure gradient. Those profiles are shown in Fig. 6. By assuming the same rotational transform profile as in the previous case in Figs 4 and 5, the obtained mode structures are shown in Fig. 7. The reason why the mode structure of the first growing mode is restricted to the inner region is that, since the average pressure gradient is equal on both sides of $r = 0.5$, the interchange mode is considered to be excited in the weaker shear region. It is interesting that the mode structure with the sharp decrease at $r = r_s$ is observed even though the pressure is completely flat in a region with a finite width around the mode resonant surface. This confirms our conjecture that the locally steep profile of the mode structure such as that in Figs 5 and 7 is caused only by the profile of the magnetic shear, not any more by the pressure profile. We note that a non-resonant feature is seen in the radial mode structure for the second growing mode in Fig. 5(b) and the first growing mode for the second pressure profile (27) in Fig. 7(b), i.e. the peak is shifted from the resonant surface. This clearly shows that the unstable mode is driven by the negative pressure gradient at locations

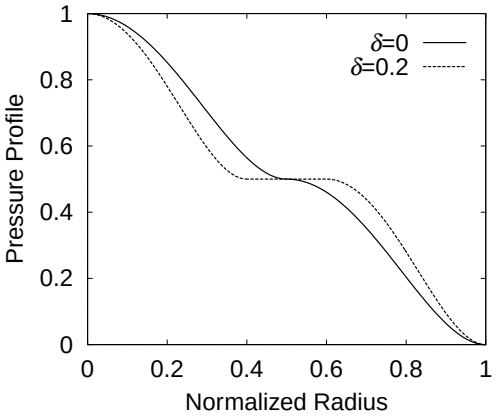

Figure 6. Pressure profiles with locally flat regions around the mode resonant surface. The solid curve corresponds to Eq. (26) and the broken curve to Eq. (27).

elsewhere than the resonant surface. A theoretical explanation for the appearance of the sharp decrease to zero at the resonant surface in the radial mode structure or $u(r)$ is given in the Appendix.

4.3. Behaviour of non-resonant type modes

We will show that a non-resonant type mode is also excited even if the pressure profiles do not have exactly zero gradient at the resonant surface. For small and non-zero values of p' at $r = r_s$, we discuss the transition from the resonant mode to the non-resonant one. We assume $p = p_0(1-r^2)^\alpha$, where α is changed from 4 to 14 (Fig. 8). The profile of the rotational transform is fixed as $\iota = 0.4 + 0.2r^2$, where the resonant surface for the $(2,1)$ mode exists at $r_s = \sqrt{2}/2$. Figure 8 shows that the mode structure gradually changes from a resonant one to a non-resonant type one. Particularly the $\alpha = 14$ case shows that the peak of the radial mode structure exists at a position different from the resonant surface, which is considered as a non-resonant feature. It does have a step function structure instead of a peak at the mode resonant surface for the nearly marginal beta value. In other words, the driving force to the instability comes from the largest pressure gradient region different from the resonant surface. From the sharp decrease of u to zero at the resonant surface in the $\alpha = 14$ case, it is considered that the pressure has almost no effect on the mode structure at the resonant surface, since p' and p'' are negligibly small. In the $\alpha = 10$ case, the mode structure has maximum value at the resonant surface; however, there exists another broad peak on the inner side of the

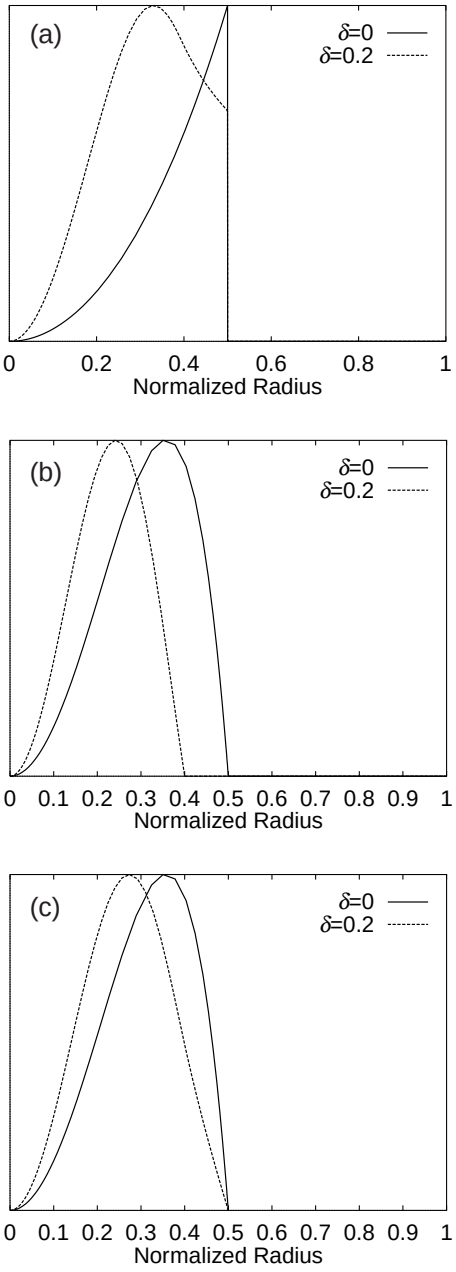

Figure 7. (a) Radial mode structures of the $(2,1)$ mode for the pressure profiles corresponding to Eq. (26) ($\delta = 0$ curves) and to Eq. (27) ($\delta = 0.2$ curves). Both curves show the radial mode structure of each first growing mode. Here all the perturbed functions are shown: (a) $\tilde{u}$, (b) $\tilde{p}$, (c) $\tilde{\psi}$.

resonant surface. In addition, the growth rate vanishes without the tail near the beta limit (Fig. 8(b)). In the $\alpha = 8$ case, the situation is more ambiguous. The mode structure has a maximum value at the resonant surface and has no other peak. However, the dependence of γ on β near the beta limit is different

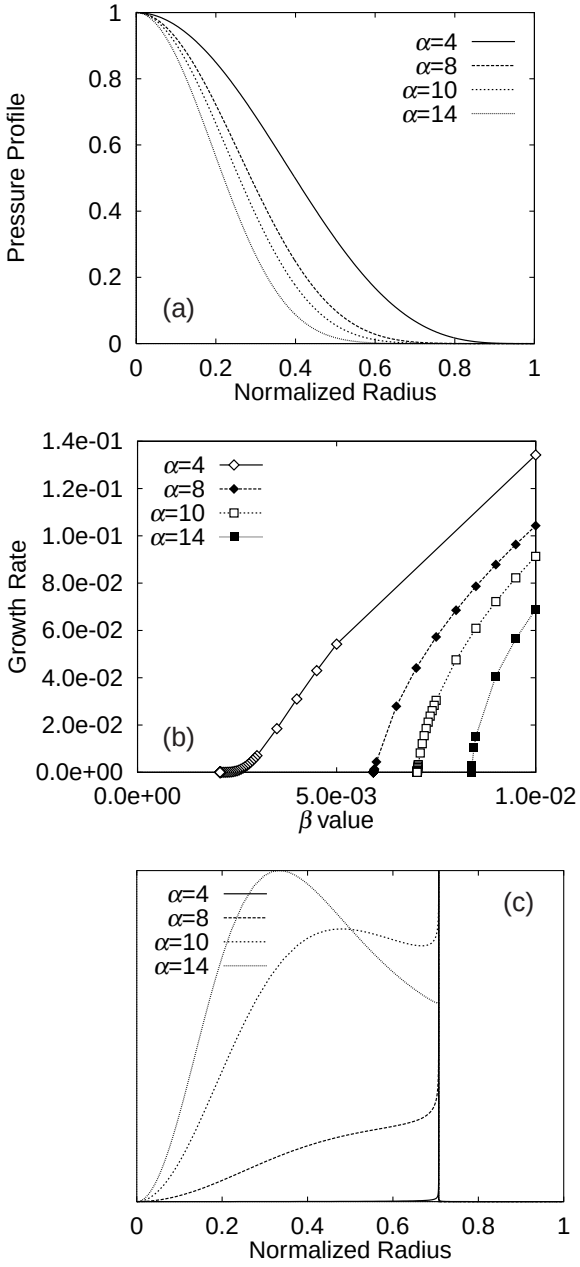

Figure 8. (a) Pressure profiles given by $p = p_0(1-r^2)^\alpha$ for $\alpha = 4$, 8, 10 and 14. (b) Dependence of the growth rate on the central beta value β_0 for different α. (c) Radial mode structures near the beta limit for different α. The height of the mode structure is normalized to its own maximum value.

from the standard resonant mode. Thus, the properties of the cases with $\alpha = 8$ and 10 seem to be intermediate between the resonant and non-resonant type modes. For the $\alpha = 4$ case, a clear feature of the resonant mode is seen, i.e. the small growth rate regime is extended to the low beta side in β–γ space, and the nearly marginal mode structure is highly localized at the resonant surface. For comparison, the beta limit given by the Suydam criterion is calculated for each equilibrium in Fig. 8. Table 1 shows both the beta limit obtained from the Suydam criterion (21) at the resonant surface of the $(2,1)$ mode, β_S, and the one shown in Fig. 8(b), β_n. From Table 1, in the cases with $\alpha \geq 8$, the non-resonant type $(2,1)$ modes are unstable even when the central beta value is smaller than the Suydam limit. The beta limit in the case of $\alpha = 4$ almost coincides with the Suydam limit since the radial mode structure is highly localized around the resonant surface.

Table 1. Comparison between the marginal beta values from the Suydam criterion, β_S, and the ones shown in Fig. 8(b), β_n. The equilibrium pressure gradient at the resonant surface is also shown.
(The pressure is normalized by the central value and the radial variable by the minor radius of the plasma column.)

α	β_S	β_n	p'
4	1.91×10^{-3}	2.07×10^{-3}	-0.707
8	1.53×10^{-2}	5.92×10^{-3}	-8.84×10^{-2}
10	4.90×10^{-2}	7.02×10^{-3}	-2.76×10^{-2}
14	0.560	8.39×10^{-3}	-2.41×10^{-3}

Finally, we considered a reversed shear profile, which will be realized in the high beta equilibrium of a toroidal stellarator. Here we assume a cylindrical plasma with $\iota' < 0$ in the central region and $\iota' > 0$ in the outer region. We also assume the following profile of the rotational transform:

$$\iota = \iota(0) + \sigma r^2 - \lambda \exp\left[-\frac{1}{2}\left(\frac{r - r_c}{W}\right)^2\right] \qquad (28)$$

where σ is the previously defined shear parameter, r_c is the parameter for the minimum point of $\iota(r)$ and W denotes the characteristic width of the non-monotonic region of $\iota(r)$. Here $\sigma = 0.2$, $r_c = 0.5$, $W = 0.15$ and $\lambda = 0.2$ are chosen as an example. The pressure profile is again assumed to be parabolic, $p = p_0(1 - r^2)$. We have calculated two cases which are parameterized as follows. One is the double resonant case, $\iota(0) = 0.6$, in which the radial positions of the two resonant surfaces for the $(2,1)$ mode are at 0.35 and 0.59, where the beta limits predicted from the Suydam criterion (21) are 6.61×10^{-3} and 8.25×10^{-3}, respectively. The other is the non-resonant case, $\iota(0) = 0.66$, in which the rotational transform has its minimum value 0.508 at $r = 0.478$.

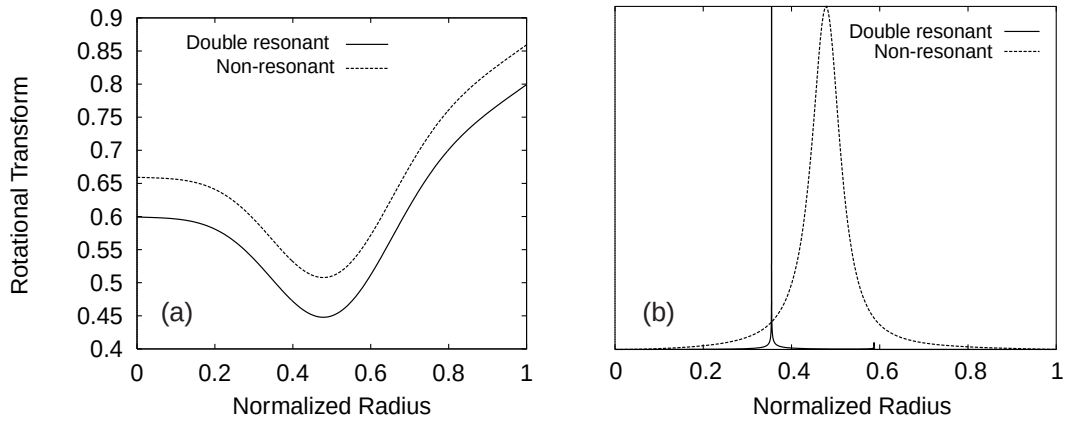

Figure 9. (a) Profiles of the rotational transform for $\iota(0) = 0.6$, $\sigma = 0.2$, $r_c = 0.5$, $W = 0.15$, $\lambda = 0.2$ (double resonance) and $\iota(0) = 0.66$, $\sigma = 0.2$, $r_c = 0.5$, $W = 0.15$, $\lambda = 0.2$ (no resonance). (b) Radial mode structure of the $(2, 1)$ mode near the beta limit; $\beta_0 = 7.79 \times 10^{-3}$ for the double resonant case, or $\beta_0 = 4.87 \times 10^{-4}$ for the non-resonant case.

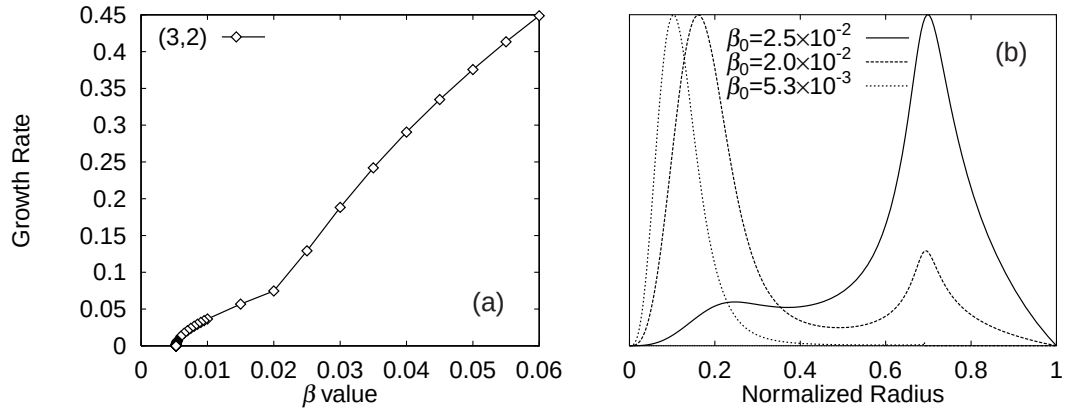

Figure 10. (a) Growth rate as a function of β_0. (b) Radial mode structures for $\beta_0 = 2.5 \times 10^{-2}$, 2.0×10^{-2} and 5.3×10^{-3}. The beta limit is estimated as 5.27×10^{-3}, which is lower than the Suydam limit at the resonant surface of the $(3, 2)$ mode.

The profiles of both the rotational transform and the nearly marginal mode structures are shown in Fig. 9.

In the double resonant case the radial mode structure is localized dominantly at the inner resonant surface. The reason is that, since the beta limit from the Suydam criterion is lower at the inner resonant surface than that at the outer one, the pressure driven mode is more unstable at the inner resonant surface. In the non-resonant case the radial mode structure is restricted near the minimum point of the rotational transform and the beta limit is much lower than that in the double resonant case. It can be interpreted that, since the pressure driven mode is excited near the minimum point of ι in the non-resonant case, which is fairly close to $\iota = 0.5$, the stabilizing magnetic shear is very weak there. On the other hand, the resonant mode is localized at the resonant surface where the magnetic shear is relatively strong in the double resonant case, thus the beta limit becomes higher than that in the non-resonant case.

We have also calculated the $(3, 2)$ mode in the non-resonant case with the rotational transform shown by the dashed curve in Fig. 9(a). This mode has one resonant surface at $r_s = 0.691$, where the beta limit from the Suydam criterion is $\beta_S = 8.28 \times 10^{-3}$. The numerical results are shown in Fig. 10. Figure 10(a) shows a transition in the growth rate depending on β_0, which occurs at $\beta_0 \sim 0.02$. This transition is understood from the mode structures shown in Fig. 10(b). The maximum point of the unstable mode structure is located at the resonant surface for

$\beta_0 \gtrsim 0.025$. However, it moves to the inner weak shear region for the non-resonant type mode with $\beta_0 \lesssim 0.02$. This type of mode structure has a small peak at r_s near the beta limit; however, it does not decrease to zero at the resonant surface as shown previously, since the pressure gradient is not small there.

5. Concluding remarks

We have clarified the properties of the non-resonant pressure driven instabilities and their relation to the resonant instabilities in the cylindrical plasma model. The behaviour of the non-resonant type mode depends strongly on the profile of both the pressure and the rotational transform. For some cases the instability has a mixed character between the resonant and non-resonant modes. In addition, a transition from a resonant mode to a non-resonant type mode occurs when the pressure gradient is increased in the central region or the pressure profile becomes peaked.

First we have solved the eigenmode equation analytically with respect to the perturbed stream function for an equilibrium with a constant rotational transform and a parabolic pressure profile. It is noted that the non-resonant mode has a global structure, and the dependence of γ on β is parabolic (Eq. (18)). In this case, it can be shown that the mode with the fewest node numbers has the larger growth rate, and the higher harmonic mode with the same helicity has the higher beta limit.

With the numerical calculations, it is shown that the growth rate of the non-resonant mode decreases to zero without the tail near the beta limit, while the resonant mode has a fairly wide small growth rate regime expressed as $\gamma \propto \exp[-\text{const}/\sqrt{\beta_0 - \beta_S}]$ [3], where β_S denotes the central beta value given by the Suydam criterion. A physical interpretation is as follows. Although the resonant mode becomes localized at the resonant surface with the decrease of beta value, the non-resonant mode does not have such a surface in the plasma column. Therefore, the free energy necessary to excite the non-resonant modes is always finite, since the parallel wavenumber along the magnetic field lines is also finite. Thus, the growth rate decreases to zero without the tail near the beta limit. In the resonant case, since the higher harmonic modes have larger poloidal and toroidal wavenumbers than the fundamental mode, they can be more localized in the radial direction. Thus, the growth rates at the same beta value are larger than that of the fundamental mode. However, all modes can be highly localized at the resonant surface as the central beta value decreases, the beta limit does not depend on the mode numbers and agrees with the Suydam limit. On the contrary, in the non-resonant case, since the parallel wavenumber of the higher harmonic mode becomes larger than that of the fundamental mode, the higher harmonics need more energy for excitation in the low beta regime. Thus, the beta limit of the non-resonant mode with a higher harmonic mode number is larger than that of the fundamental mode.

When the pressure profile becomes locally flattened with a width of W around the resonant surface, the resonant mode shows a non-resonant feature. The beta limit in this case is increased in the small flattening region. The marginal mode structure is quite different from the case with $W = 0$, i.e. it is restricted to one side of the resonant surface and the growth rate decreases to zero without a tail when β_0 approaches the marginal value. It is noted that this non-resonant feature also appears in case of a non-zero but small pressure gradient at the resonant surface.

In Heliotron-E, when the beta value is increased, the central rotational transform is increased and the profile becomes non-monotonic. We have studied this situation by changing the rotational transform artificially. Even if there is no resonant surface for the $(2, 1)$ mode, when the minimum of the rotational transform, ι_{min}, is close to 0.5, the non-resonant $(2, 1)$ mode becomes unstable, which is independent of the Suydam criterion. When ι_{min} is less than 0.5, the double resonant mode becomes unstable. In addition, the non-resonant type $(3, 2)$ mode is unstable below the Suydam limit at the $\iota = 2/3$ surface. In this case a radial mode structure is observed in the central region when $\iota(0)$ is sufficiently close to 2/3.

Appendix

Behaviour of eigenfunctions in a resonant layer with a negligibly small pressure gradient

By introducing the variable $\xi = u/r$, the eigenmode equation (16) is written in the Sturmian form as

$$\frac{d}{dr}\left(p(r)\,\frac{d\xi}{dr}\right) - q(r)\xi = 0 \tag{29}$$

where

$$p(r) = r^3[\gamma^2 + (n - m\iota)^2]$$

$$q(r) = r\big\{(m^2-1)[\gamma^2 + (n - m\iota)^2] + (3m\iota' r + m\iota'' r^2)(n - m\iota) - D_s m^2\big\}.$$

Here we consider a resonant layer satisfying $|r - r_s| = |x| \sim \epsilon$. Since our interest is in the small growth rate limit, $\gamma \sim \epsilon$ is also assumed. Under these assumptions, if we assume $p' \simeq 0$ in the resonant layer, the second term in Eq. (29) becomes negligible and

$$\frac{d}{dr}\left(p(r)\,\frac{d\xi}{dr}\right) = 0 \tag{30}$$

decides the behaviour of the eigenfunction $\xi(r)$ in the resonant layer. It is noted that Eq. (30) is exactly the same as that given by Rosenbluth, Dagazian and Rutherford for the $m = 1$ internal kink mode in a cylindrical tokamak [15]. They gave the solution

$$\xi = \frac{1}{2}\,\xi_a\left[1 - \frac{2}{\pi}\tan^{-1}\left(\left|\frac{m\iota'}{\gamma}\right| x\right)\right] \tag{31}$$

for the boundary conditions $\xi \to \xi_a$ as $x \to -\infty$ and $\xi \to 0$ as $x \to \infty$. Since $m\iota'/\gamma \sim O(\epsilon^{-1})$, the eigenfunction ξ has the largest gradient at $r = r_s$ and has a step function structure near the resonant surface. Further, since $u \simeq r_s\xi$ in the neighbourhood of the resonant layer, this type of solution may explain the behaviour of the sharp decrease to zero of the eigenfunction with the largest growth rate near the resonant surface $r = r_s$ for $\gamma \to 0$.

References

[1] Shafranov, V.D., Yurchenko, E.I., Sov. Phys.–JETP **26** (1968) 682.
[2] Shafranov, V.D., Phys. Fluids **26** (1983) 357.
[3] Sugama, H., Wakatani, M., J. Phys. Soc. Jpn. **58** (1989) 1128.
[4] Nakamura, Y., et al., Fusion Technol. **19** (1991) 217.
[5] Fu, G.Y., et al., Phys. Fluids B **4** (1992) 1401.
[6] Wakatani, M., et al., in Plasma Physics and Controlled Nuclear Fusion (Proc. 9th Int. Conf. Toki, 1998), Natl Inst. for Fusion Science, Nagoya (in press) Paper OP-5.
[7] Ichiguchi, K., Nakamura, Y., Wakatani, M., Nucl. Fusion **31** (1991) 2073.
[8] Carreras, B.A., Lynch, V.E., Zushi, H., Ichiguchi, K., Wakatani, M., Phys. Plasmas **5** (1998) 3700.
[9] Zushi, H., et al., in Fusion Energy 1996 (Proc. 16th Int. Conf. Montreal, 1996), Vol. 2, IAEA, Vienna (1997) 143.
[10] Strauss, H.R., Plasma Phys. **22** (1980) 733.
[11] Goedbloed, J.P., Sakanaka, P.H., Phys. Fluids **17** (1974) 908.
[12] Furth, H.P., Killeen, J., Rosenbluth, M.N., Phys. Fluids **6** (1963) 459.
[13] Nakamura, Y., Wakatani, M., Hegna, C.C., Bhattacharjee, A., Phys. Fluids B **2** (1990) 2528.
[14] Nührenberg, J., Zille, R., Phys. Lett. **114A** (1986) 129.
[15] Rosenbluth, M.N., Dagazian, R.Y., Rutherford, P.H., Phys. Fluids **16** (1973) 1894.

(Manuscript received 8 February 1999
Final manuscript accepted 5 August 1999)

E-mail address of M. Wakatani:
wakatani@energy.kyoto-u.ac.jp

Subject classification: C0, St